Influence of chest compression artefact on capnogram-based ventilation detection during out-of-hospital cardiopulmonary resuscitation.

Mikel Leturiondo[a], Sofía Ruiz de Gauna[a,*], Jesus M. Ruiz[a], J. Julio Gutiérrez[a], Luis A. Leturiondo[a], Digna M. González-Otero[a], James K. Russell[b], Dana Zive[b], Mohamud Daya[b]

Affiliation and addresses:

[a] Department of Communications Engineering. University of the Basque Country, UPV/EHU, 48013 Bilbao, Spain

[b] Department of Emergency Medicine, Oregon Health & Science University, OHSU, 97239-3098 Portland, Oregon, USA

Corresponding author:

[*] Sofía Ruiz de Gauna
email: sofia.ruizdegauna@ehu.es
Tel. : +34946017341
Fax. : +34946014259

Word counts:

Abstract: Aprox. 233 words
Paper : Aprox. 2950 words

Abstract

Background: Capnography has been proposed as a method for monitoring the ventilation rate during cardiopulmonary resuscitation (CPR). A high incidence (above 70%) of capnograms distorted by chest compression induced oscillations has been previously reported in out-of-hospital (OOH) CPR. The aim of the study was to better characterize the chest compression artefact and to evaluate its influence on the performance of a capnogram-based ventilation detector during OOH CPR.

Methods: Data from the MRx monitor-defibrillator were extracted from OOH cardiac arrest episodes. For each episode, presence of chest compression artefact was annotated in the capnogram. Concurrent compression depth and transthoracic impedance signals were used to identify chest compressions and to annotate ventilations, respectively. We designed a capnogram-based ventilation detection algorithm and tested its performance with clean and distorted episodes.

Results: Data were collected from 232 episodes comprising 52 654 ventilations, with a mean (± SD) of 227 (± 118) per episode. Overall, 42% of the capnograms were distorted. Presence of chest compression artefact degraded algorithm performance in terms of ventilation detection, estimation of ventilation rate, and the ability to detect hyperventilation.

Conclusion: Capnogram-based ventilation detection during CPR using our algorithm was compromised by the presence of chest compression artefact. In particular, artefact spanning from the plateau to the baseline strongly degraded ventilation detection, and caused a high number of false hyperventilation alarms. Further research is needed to reduce the impact of chest compression artefact on capnographic ventilation monitoring.

Keywords

Cardiopulmonary resuscitation, Advanced life support, Capnography, Ventilation, Chest compression artefact.

1. Introduction

Capnography is now considered a standard of care in advanced cardiopulmonary resuscitation (CPR)[1–3]. As emphasized in current resuscitation guidelines, advantages of capnography during CPR include assessment of the correct placement of the endotracheal tube[4], monitoring quality of chest compressions[5,6], early identification of restoration of spontaneous circulation (ROSC)[7], and determination of patient prognosis[3,8,9].

Another important role of capnography during CPR is ventilation rate monitoring to prevent inadvertent hyperventilation[8]. Guidelines recommend ventilating the lungs at approximately 10 breaths per minute. However, excessive ventilation rates are common in resuscitation. In a clinical observational study, Aufherheide et al. reported ventilation rates of 30 breaths per minute or more as a norm[10]. Subsequent clinical studies have also confirmed the tendency to ventilate with such high rates[11,12]. One animal study revealed that similar excessive ventilation rates increased intrathoracic pressures and decreased coronary perfusion pressures and survival rates[13]. Another animal study by Gazmuri et al. reported no adverse hemodynamic effects during CPR after increasing ventilation rate and tidal volume over the recommended values, although they observed a decrease in end-tidal CO2 values[14].

Current guidelines recommend using capnography during CPR to monitor ventilation rate and avoid hyperventilation. Visual inspection of the capnogram allows tracking respiratory cycles, since the onset of each ventilation causes a downstroke in the capnography waveform. Automated measurement of ventilation rate and algorithms for hyperventilation detection using capnography were first explored by Edelson et al. in 2010[15], as an alternative to customary algorithms based on the transthoracic impedance recorded through defibrillation pads[16].

Quality of the recorded capnogram is essential for a reliable analysis, either visual or automated. However, a clean capnogram, in which the different phases of the respiratory cycle are identifiable (inspiratory downstroke, inspiratory baseline, expiratory upstroke, and alveolar plateau, where end-tidal CO2 value is measured) cannot always be observed during CPR. Sources of artefact include issues related to the capnography device (occlusion in the CO2 circuit, leaking) as well as the ongoing resuscitation efforts[1,17,18]. In this study, we focused on analysing the artefact induced on the capnogram by chest compressions during CPR. This artefact appears in the form of fast oscillations at different rates and with varying amplitude superimposed on the capnogram. This phenomenon has received little attention in the literature to date. An abstract presented at the 2010 American Heart Association Resuscitation Science Symposium reported chest compression artefact presence in greater than 70% of capnograms in a sample of 210 out-of-hospital (OOH) cardiac arrest episodes[19]. To our knowledge there are no published studies that systematically analyse the morphology of this artefact. We hypothesized that chest compression artefact may impede a reliable analysis of the capnogram, compromising its application for ventilation rate monitoring.

The purpose of this study was three-fold. First, we identified capnograms distorted by chest compression artefact in a large dataset of OOH cardiac arrest episodes in order to confirm the high incidence of this artefact during CPR. Second, we characterized the morphology of chest compression artefact. Third, we assessed the impact of chest compression artefact on the reliability of automated capnogram-based guidance of ventilation rate.

2. Materials and Methods

2.1. Data collection

Data were extracted from a database of 691 OOH episodes collected between 2011 and 2016 by Tualatin Valley Fire & Rescue (TVF&R), an advanced life support first response Emergency Medical Services (EMS) agency serving eleven incorporated cities (about $1\,015\,\mathrm{km}^2$) in Oregon, USA. Episodes were collected as part of the Resuscitation Outcomes Consortium (ROC) Epidemiological Cardiac Arrest Registry. The data collection for the ROC Epistry was approved by the Oregon Health & Science University (OHSU) Institutional Review Board (ID: IRB00001736). No patient private data was required for this study.

Episodes were recorded with Heartstart MRx monitor-defibrillators (Philips, USA), equipped with real-time CPR feedback technology (Q-CPR). Capnography was acquired using sidestream technology (Microstream, Oridion Systems Ltd, Israel). Ventilation was provided with a bag-valve-mask or an advanced airway. The choices for the latter were the endotracheal tube or the King LT-D (supraglottic). Defibrillator signals used in the study were the capnogram, the compression depth (CD) signal measured by the Q-CPR chest pad, and the transthoracic impedance (TI) signal acquired from defibrillation pads.

Episodes with at least 20 min of continuous and simultaneous signals, and with a minimum of 500 chest compressions were included in the study, which yielded a total of 301 episodes.

2.2. Data annotation

Signals were reviewed and annotated using a custom-made Matlab (Mathworks, USA) program. Intervals with unreliable raw TI signal or capnogram caused by disconnections or excessive noise were discarded. For each episode, capnograms were time-shifted to compensate for the delay with respect to CD and TI signals.

Three biomedical engineers with experience in the analysis of OOH defibrillator signals participated in the annotation process. They reviewed one third of the cases jointly, and defined the annotation rules for identifying capnograms distorted by chest compression artefact, and for annotating ventilations using the TI signal. The rest of episodes were randomly split in three parts, each of them examined by a single reviewer. At the end of this process, the three experts joined again to solve by consensus undecided annotations.

Experts annotated intervals in which capnograms were distorted by chest compression artefact, with the support of the CD signal. Episodes were classified as distorted if evident chest compression artefact appeared during more than one minute of the chest compression time. In addition, they annotated the location of the artefact with respect to the respiratory phase (e.g. appearing mainly on the expiratory phase or on the inspiratory phase).

Ventilations were manually annotated using the low frequency component of the TI signal. A low-pass filter was applied to the raw TI signal to suppress fast oscillations caused by chest compressions and enhance slow fluctuations caused by ventilations. Figure 1 (top panel) shows the raw TI signal in grey with the low frequency TI component superimposed in blue. Each ventilation was annotated at the instant corresponding to a rise in each TI fluctuation (marked with a vertical dashed red line in Figure 1). The capnogram is depicted in the bottom panel to visually confirm the presence of ventilations. The resulting annotations were used as our gold standard to test the performance of the automated capnogram-based ventilation detection algorithm.

2.3. Automated capnogram-based ventilation detection algorithm

The algorithm used in this study processes the capnogram, and was designed following a finite-state-machine model. Figure 2 shows the flow chart of the algorithm (top) and the definition of the main parameters of the algorithm (bottom). Basically, the algorithm searches for an abrupt upstroke in the capnogram, t^i_{up}, which is detected when the amplitude of the capnogram exceeds a fixed threshold, Th_{amp} (mmHg). Then, the algorithm searches for an abrupt downstroke, t^i_{dw}, detected when the capnogram goes below the same threshold, Th_{amp}. To detect a ventilation, the duration of the interval $D_{\mathrm{ex}} = t^i_{\mathrm{dw}} - t^i_{\mathrm{up}}$ and the duration of the interval $D_{\mathrm{in}} = t^{i+1}_{\mathrm{up}} - t^i_{\mathrm{dw}}$ must exceed thresholds Th_{ex} and Th_{in}, respectively. If both conditions are satisfied, the ventilation is annotated at the instant when the inspiratory downstroke occurs, t^i_{dw}.

To account for observed *double ventilation* effects (Figure 2, bottom right), the algorithm discards any ventilation for which the interval D_{in} is below Th_{in}, and searches for the next downstroke and upstroke until D_{in} exceeds Th_{in}.

2.4. Data analysis

Ventilation detector performance was evaluated in terms of its sensitivity (Se) and positive predictive value (PPV). Se was defined as the proportion of annotated ventilations detected by the algorithm. PPV was the proportion of detections that were indeed annotated ventilations. We allowed a tolerance of ± 0.5 s between the detection and the annotation instant. The algorithm was trained with a subset of clean (non-distorted) episodes applying the criterion of maximum Se while assuring a PPV $> 98\%$.

In order to assess the influence of the artefact in the estimation of ventilation rate, we computed, for each episode, ventilation rate value per minute, updated every 10 s. These ventilation rate measurements were computed using the gold standard (annotated ventilations) and using the ventilations detected by our algorithm.

We also computed hyperventilation alarms from the ventilation rate per minute measurements. Results were obtained for hyperventilation thresholds set at 10, 15, and 20 min^{-1}. Then, we tested the ability of our algorithm to correctly detect hyperventilation. In this case, Se was defined as the proportion of annotated hyperventilation alarms that were given by the algorithm, and PPV as the proportion of hyperventilation alarms given that were indeed annotated.

Data were reported as mean ($\pm$ SD) if they passed Lilliefors normality test, and as median (IQR) otherwise. Distribution of Se and PPV per record, and distributions of the percent error in the estimation of ventilation rate were depicted with boxplots.

Finally, the morphology of the artefact was characterized by the spectral analysis of clean and distorted capnograms. We computed the power spectral density (PSD) of the capnogram and located the frequency components associated with the artefact. We used the chest compression rate derived from the CD signal as reference.

3. Results

From the original dataset of 301 episodes, 69 were discarded (23%) due to unreliable capnogram or TI signals. Reasons for elimination were: permanent signal disconnection or saturation, capnogram below 5 mmHg along the entire episode or without variations associated to respiratory cycles, and failure to observe ventilation waves in the filtered TI signal. Thirty-two episodes out of 69 were discarded due to unreliable capnogram, 20 to unreliable TI signal, and 17 due to unreliability of both signals. Overall, unrealiable capnograms were found in 16.3% of the episodes included in the study. The remaining 232 episodes had a mean duration of 31 ($\pm$9.5) min, with a mean of 2301 ($\pm$1230) annotated chest compressions per episode.

Ninety-eight episodes (42%) were annotated as distorted. We classified the artefact into three types: observed primarily in the expiratory plateau of the capnogram (type I), in the baseline (type II), and spanning from the plateau to the baseline (type III). Figure 3A shows examples of capnogram intervals observed during chest compressions.

We conducted an spectral analysis to characterize the waveform nature of the chest compression artefact. This is illustrated in Figure 3B, which depicts an interval of corrupted capnogram (top), the concurrent CD signal (middle) and the PSD of the capnogram. A primary peak is clearly observed at 1.94 Hz, with no peaks at frequencies multiple of this fundamental frequency, i.e. no harmonic components. This value corresponds to the fundamental frequency of the artefact, f_{art}, and matches the average compression rate in that interval ($f_{art} \cdot 60 = 116$ compressions per minute). This proves that the artefact is mainly sinusoidal and that it is directly caused by chest compressions during CPR.

Table 1 shows the incidence of each artefact type in relation to the airway system used in each case. Type I artefact was annotated in 48% of the distorted episodes, type II in 21%, and type III in 31% of the episodes. Artefact did not appear in the episodes where bag-valve-mask was used. However, all types of artefact appeared in every advanced airway type, although the incidence was higher for supraglottic cases. Incidence of type III artefact (plateau to baseline) was more prevalent in endotracheal intubation, and incidence of type I (plateau) was more prevalent in supraglottic.

A total number of 52 654 ventilations were annotated, with a mean of 227 ($\pm$ 118) ventilations per episode. Clean episodes comprised 30 814 ventilations, and distorted episodes 21 840 ventilations (Type I: 10 119, Type II: 5 228, and Type III: 6 493).

The ventilation detection algorithm was trained with a subset of 30 clean episodes. Optimal values for algorithm parameters Th_{ex} and Th_{in} were achieved for a Se/PPV of 99.8/99.0%. Figure 4A shows the performance results of the ventilation detector algorithm using the test subset. Boxplots depict the distribution of the Se and PPV calculated per episode. For the whole test subset, median (IQR) Se was 99.4 (97.8 – 100)%, and PPV was 98.6 (96.4 – 99.5)%. For the distorted test subset, Se was 97.4 (90.3 – 99.3)%, and PPV was 95.6 (85.9 – 98.3)%. For type III episodes, Se decreased to 85.2 (59.2 – 92.7)%, and PPV to 76.9 (47.0 – 90.5)%. Figure 4B shows the distribution of the percent error in the estimation of the ventilation rate. For the clean episodes, median error was -0.6 (-1.9 – 0.0)%. For the distorted test subset, error was -6.1 (-16.9 – 1.2)%. For type III episodes, error was -18.8 (-39.1 – 6.7)%.

Table 2 shows the algorithm performance in the detection of hyperventilation alarms. Hyperventilation was accurately detected regardless of the hyperventilation threshold in the clean episodes. Performance decreased in the distorted group, particularly with respect to PPV. Detection of hyperventilation was particularly compromised in the presence of type III artefact.

4. Discussion

Monitoring ventilation rate is one of the recommended uses of capnography waveform during CPR. However, the presence of high-frequency oscillations in the capnogram during chest compressions may compromise the interpretation of the signal.

Our findings demonstrated the impact of this artefact on the reliability of capnogram guided ventilation monitoring. Detection of ventilations was accurate for clean episodes (Se and PPV were above 95% for all episodes), but algorithm performance significantly decreased when artefact was present. For some of the cases Se and PPV were well below 80%, and errors in the measurement of ventilation rate were as high as 50%. This means that, with such a degree of distortion, reliable ventilation rate guidance would not be feasible for those patients. These poor results were mainly attributable to type III artefact, annotated in 31% of the distorted episodes (13% of all episodes). Oscillations disturbing the capnogram from the plateau to the baseline impeded the reliable detection of CO2 concentration changes associated to a true ventilation.

Ventilation rates above the recommended 10 breaths per minute were common in our database, with a 56.4% of annotated hyperventilation alerts. Regardless the established hyperventilation threshold, sensitivity for alarm detection was high for clean and also for distorted cases in general. However, the presence of artefact caused an increase in the number of false hyperventilation alarms, and this was especially noticeable for type III cases. This shows the tendency of the algorithm to overestimate ventilation rate, as the presence of artefact caused many false ventilation detections.

The incidence and nature of the artefact has not been studied in the literature. To our knowledge, only one prior study has examined the impact of chest compression artefact on the capnogram during OOH CPR[19]. In this study only published as a conference abstract, Idris et al. reported that 73% (154/210) of the episodes were disturbed by oscillations due to chest compressions. In our study, we found a lower incidence (42%) of corrupted capnograms for a similar number of OOH records (232 vs. 210). This difference could be partly explained by different annotation criteria for corrupted episodes. Nevertheless, characterization and analysis of potential effects of such artefact on the interpretation of the capnogram are warranted.

We quantitatively confirmed the pure sine wave nature of the chest compression artefact, with a frequency matching the chest compression rate. This suggests that the artefact is directly caused by chest compressions during CPR. We consider that chest compressions cause incidental ventilations of sufficient volume to alter the CO2 concentration sensed by the capnography device, distorting the capnnogram. Few studies have documented low ventilation volumes incidental to chest compressios[20,21]. These volumes were lower than the anatomical dead space, and therefore generated limited gas exchange. Additionally, in our study artefact appeared when advanced airway was used, and was more predominant for supraglottic (King LT-D). However, the most compromising type III artefact was more pronounced with endotracheal intubation. Differences in the seal position and the cuff size might explain this, but more studies are necessary to interpret these findings.

One of the hypothesis we will explore in further research is that automatic ventilation detection would improve if the artefact could be successfully removed from the capnogram. Designing filtering approaches for this aim will be our next step, exploring different alternatives. We will focus on the preservation of the capnogram waveform after filtering in order to allow the clinical interpretation of the signal.

Our study has several limitations. First, almost a quarter of episodes were discarded due to poor signal quality. Unreliable capnogram represented the 10% of the study dataset. Recordings of unreliable capnograms would limit its use to determine ventilation rate. In addition, our gold standard for ventilation detection was derived from the TI signal, and the annotation of TI fluctuations caused by ventilations is not straightforward during CPR. We had to discard several episodes because of unreliable TI signal (noisy, disconnections) and for those included in the study, filtering was needed to remove the artefact due to chest compressions from the TI signal. Unfortunately, no other reference signal (such as airway pressure or volume) was available to be used as an alternative gold standard. The inability to control for tidal volume was thus a clear limitation of the study. Another limitation is that ventilations corresponding with capnogram amplitudes below the algorithm amplitude threshold (3 mmHg) could not be detected. However, in our data that was rarely observed. Finally, data came from a single EMS system and so results may not be generalizable. Further studies are needed to clarify our findings with other EMS agencies and monitor-defibrillators.

5. Conclusions

The important role of capnography waveform in ventilation rate monitoring and hyperventilation prevention during CPR is compromised by the high-incidence of chest compression artefact. Among the different locations in which it may present, artefact spanning from the plateau to the baseline strongly affected ventilation detection, and caused a high number of false hyperventilation alarms. Further research could explore filtering techniques to suppress chest compression artefact in order to improve ventilation monitoring for corrupted capnograms.

6. Conflict of interest

The authors declare no conflicts of interest.

Acknowledgements

This work received financial support from the Basque Government (Basque Country, Spain) through the project IT1087-16 and the predoctoral research grant PRE-2016-1-0104. The authors thank the TVF&R EMS providers for collecting the data used in this study.

References

[1] Pantazopoulos C, Xanthos T, Pantazopoulos I, Papalois A, Kouskouni E, Iacovidou N. A review of carbon dioxide monitoring during adult cardiopulmonary resuscitation. Heart, Lung and Circulation 2015;24(11):1053–1061.

[2] Meaney PA, Bobrow BJ, Mancini ME, et al. Cardiopulmonary resuscitation quality: improving cardiac resuscitation outcomes both inside and outside the hospital: a consensus statement from the American Heart Association. Circulation 2013;128(4):417–435.

[3] Kodali BS, Urman RD, et al. Capnography during cardiopulmonary resuscitation: current evidence and future directions. Journal of emergencies, trauma, and shock 2014;7(4):332.

[4] Silvestri S, Ralls GA, Krauss B, et al. The effectiveness of out-of-hospital use of continuous end-tidal carbon dioxide monitoring on the rate of unrecognized misplaced intubation within a regional emergency medical services system. Annals of emergency medicine 2005;45(5):497–503.

[5] Ditchey RV, Winkler JV, Rhodes CA. Relative lack of coronary blood flow during closed-chest resuscitation in dogs. Circulation 1982;66(2):297–302.

[6] Qvigstad E, Kramer-Johansen J, Tømte Ø, et al. Clinical pilot study of different hand positions during manual chest compressions monitored with capnography. Resuscitation 2013;84(9):1203–1207.

[7] Pokorná M, Nečas E, Kratochvíl J, Skřipskỳ R, Andrlík M, Franěk O. A sudden increase in partial pressure end-tidal carbon dioxide (PETCO2) at the moment of return of spontaneous circulation. The Journal of emergency medicine 2010;38(5):614–621.

[8] Soar J, Nolan JP, Böttiger BW, et al. European Resuscitation Council guidelines for resuscitation 2015. Section 3. Adult advanced life support. Resuscitation 2015;95:100–147.

[9] Touma O, Davies M. The prognostic value of end tidal carbon dioxide during cardiac arrest: a systematic review. Resuscitation 2013;84(11):1470–1479.

[10] Aufderheide TP, Lurie KG. Death by hyperventilation: a common and life-threatening problem during cardiopulmonary resuscitation. Critical care medicine 2004;32(9):S345–S351.

[11] O'Neill JF, Deakin CD. Do we hyperventilate cardiac arrest patients? Resuscitation 2007;73(1):82–85.

[12] Maertens VL, De Smedt LE, Lemoyne S, et al. Patients with cardiac arrest are ventilated two times faster than guidelines recommend: an observational prehospital study using tracheal pressure measurement. Resuscitation 2013;84(7):921–926.

[13] Aufderheide TP, Sigurdsson G, Pirrallo RG, et al. Hyperventilation-induced hypotension during cardiopulmonary resuscitation. Circulation 2004;109(16):1960–1965.

[14] Gazmuri RJ, Ayoub IM, Radhakrishnan J, Motl J, Upadhyaya MP. Clinically plausible hyperventilation does not exert adverse hemodynamic effects during CPR but markedly reduces end-tidal PCO 2. Resuscitation 2012; 83(2):259–264.

[15] Edelson DP, Eilevstjønn J, Weidman EK, Retzer E, Hoek TLV, Abella BS. Capnography and chest-wall impedance algorithms for ventilation detection during cardiopulmonary resuscitation. Resuscitation 2010; 81(3):317–322.

[16] Alonso E, Ruiz J, Aramendi E, et al. Reliability and accuracy of the thoracic impedance signal for measuring

cardiopulmonary resuscitation quality metrics. Resuscitation 2015;88:28–34.

[17] Takla G, Petre JH, Doyle DJ, Horibe M, Gopakumaran B. The problem of artifacts in patient monitor data during surgery: a clinical and methodological review. Anesthesia & Analgesia 2006;103(5):1196–1204.

[18] Herry CL, Townsend D, Green GC, Bravi A, Seely AJE. Segmentation and classification of capnograms: application in respiratory variability analysis. Physiological measurement 2014;35(12):2343.

[19] Idris AH, Daya M, Owens P, et al. High incidence of chest compression oscillations associated with capnography during out-of-hospital cardiopulmonary resuscitation. Circulation 2010;122:A83.

[20] Idris AH, Banner MJ, Wenzel V, Fuerst RS, Becker LB, Melker RJ. Ventilation caused by external chest compression is unable to sustain effective gas exchange during CPR: a comparison with mechanical ventilation. Resuscitation 1994;28(2):143–150.

[21] Vanwulpen M, Wolfskeil M, Duchatelet C, Monsieurs K, Idrissi SH. Quantifying inspiratory volumes generated by manual chest compressions during resuscitation in the prehospital setting. Resuscitation 2017;118:e18.

Figure Legends

Figure 1 Example of ventilations annotated using the low frequency component of the TI signal (top panel, blue line). This signal was obtained after low pass filtering the raw TI signal (top panel, grey line). Each ventilation was identified at the instant corresponding to a rise in each TI fluctuation (vertical dashed red lines). The capnogram (bottom panel) is depicted with the annotations to visually confirm ventilations at the instants where CO2 concentration rapid decays to zero.

Figure 2 Flow chart of the ventilation detector (top). Main parameters of the algorithm (bottom). Capnogram ascents and descents crossing the shadowed area (amplitude threshold) are depicted with dashed/dotted lines. Downward arrow marks the position of the detected ventilation.

Figure 3 (A) Examples of chest compression artefact observed in OOH capnograms during chest compressions: clean capnogram; Type I artefact, located in the plateau; Type II, located in the baseline; Type III, spanning from the plateau to the baseline. (B) Spectral characterization of chest compression artefact in a distorted capnogram (top). CD signal, with average chest compression rate of 116 compressions per minute (middle). PSD of the distorted capnogram (bottom): the observed single peak corresponds to the fundamental frequency of the artefact, i.e. a sine wave superimposed to the lower frequency capnogram waveform.

Figure 4 (A) Performance of the ventilation detector algorithm. (B) Distribution of the error in the estimation of ventilation rate. Results are provided globally and for the different subgroups. The boxes show the median and IQR and the whisker shows the last datum within the $\pm 1.5\,$IQR. Outliers are represented by dots.

Table Legends

Table 1	Distribution of episodes according to artefact classification and type of ventilation.
Table 2	Algorithm performance (Se and PPV) in the detection of hyperventilation alarms; n (total) is the number of ventilation rate per minute measurements annotated in the test subset, and n is the number of annotated ventilation rate per minute measurements above the hyperventilation threshold.

Episodes	Ventilation type				
	BVM	**ETT**	**SGA**	**NA**	**Total**
Total	7	149	73	3	232
Clean	7	90	35	2	134
Distorted	0	59 (39.6%)[a]	38 (52.1%)[a]	1	98 (42.2%)[a]
Type I	0	19 (32.2%)[b]	28 (73.7%)[b]	0	47 (47.9%)[b]
Type II	0	15 (25.4%)[b]	6 (15.8%)[b]	0	21 (21.4%)[b]
Type III	0	25 (42.4%)[b]	4 (10.5%)[b]	1	30 (30.7%)[b]

BVM: bag-valve-mask; ETT: endotracheal tube; SGA: supraglottic airway.
NA not available
[a] Referred to the total number of episodes in the category (column)
[b] Referred to the total number of distorted episodes in the category (column)

Table 1: Distribution of episodes according to artefact classification and type of ventilation.

Group	n (total)	Alarms (>10 min^{-1})			Alarms (>15 min^{-1})			Alarms (>20 min^{-1})		
		n	**Se(%)**	**PPV(%)**	**n**	**Se(%)**	**PPV (%)**	**n**	**Se(%)**	**PPV(%)**
Total	31 760	17 901	99.1	92.6	8 966	98.1	87.2	3 567	95.1	86.8
Clean	17 413	10 511	99.7	98.0	5 710	99.5	96.8	2 502	97.7	95.1
Distorted	14 347	7 390	98.2	85.8	3 256	95.7	73.9	1 065	88.8	70.9
Type I	7 167	3 398	98.9	90.8	1 275	95.9	79.5	431	88.4	82.5
Type II	2 826	1 837	99.8	96.6	1 120	99.2	92.1	355	97.2	86.0
Type III	4 354	2 155	95.5	72.1	861	90.9	53.2	279	78.9	46.6

Table 2: Algorithm performance (Se and PPV) in the detection of hyperventilation alarms; n (total) is the number of ventilation rate per minute measurements annotated in the test subset, and n is the number of annotated ventilation rate per minute measurements above the hyperventilation threshold.

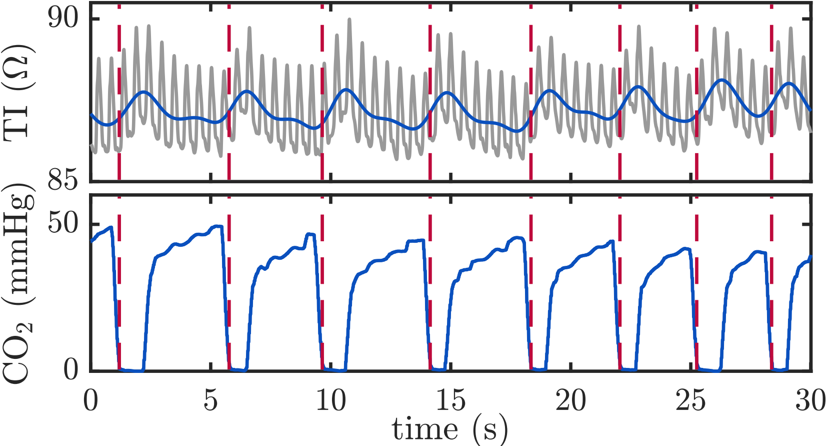

90
TI (Ω)
85
50
CO_2 (mmHg)
0
0
5
10
15
20
25
30
time (s)

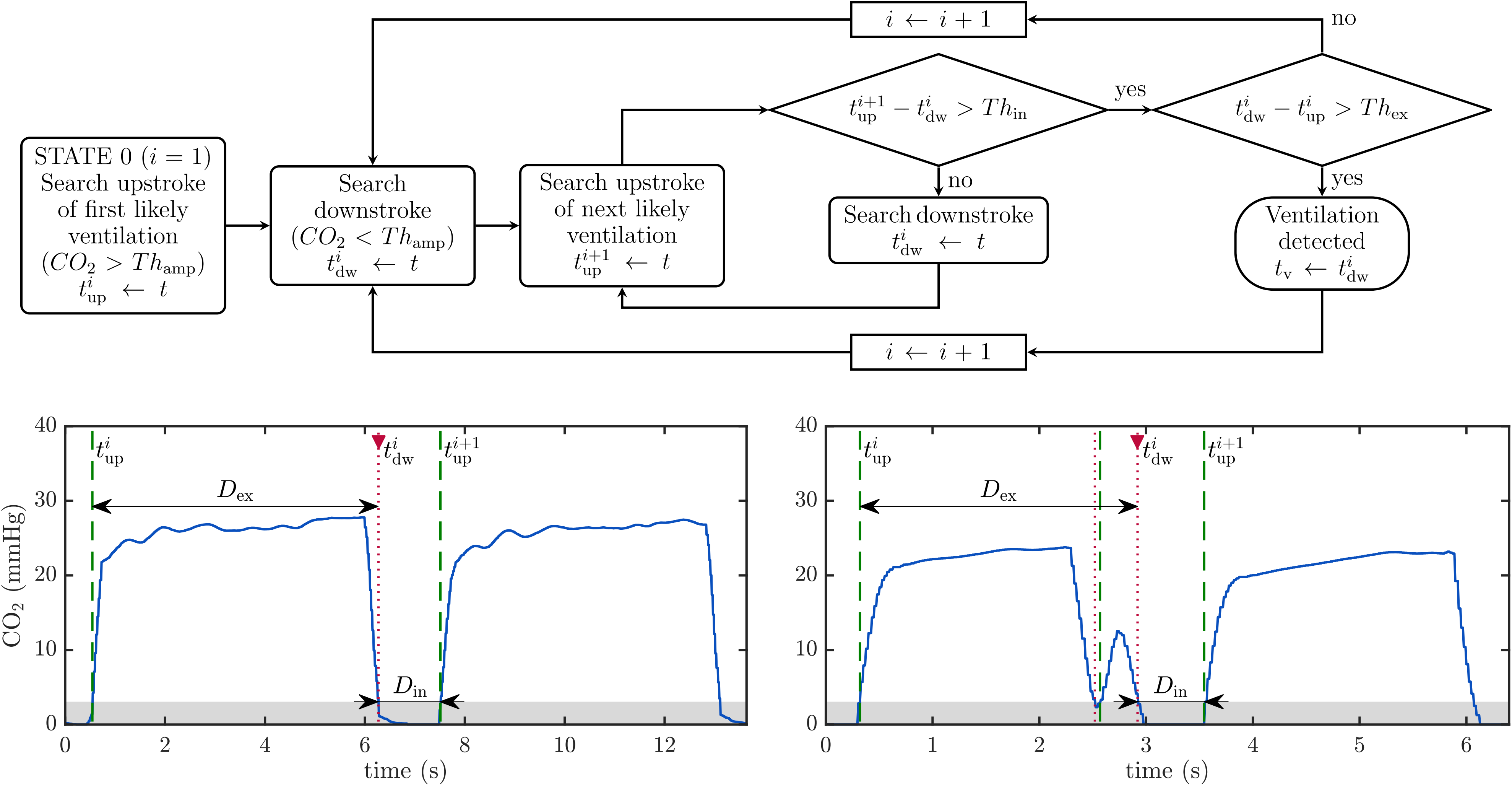

STATE 0 ($i = 1$)
Search upstroke of first likely ventilation
($CO_2 > Th_{amp}$)
$t^i_{up} \leftarrow t$
Search downstroke
($CO_2 < Th_{amp}$)
$t^i_{dw} \leftarrow t$
Search upstroke of next likely ventilation
$t^{i+1}_{up} \leftarrow t$
$t^{i+1}_{up} - t^i_{dw} > Th_{in}$
yes
no
Search downstroke
$t^i_{dw} \leftarrow t$
$t^i_{dw} - t^i_{up} > Th_{ex}$
no
yes
Ventilation detected
$t_v \leftarrow t^i_{dw}$
$i \leftarrow i + 1$
$i \leftarrow i + 1$
CO_2 (mmHg)
time (s)
time (s)
t^i_{up}
t^i_{dw}
t^{i+1}_{up}
D_{ex}
D_{in}
t^i_{up}
t^i_{dw}
t^{i+1}_{up}
D_{ex}
D_{in}

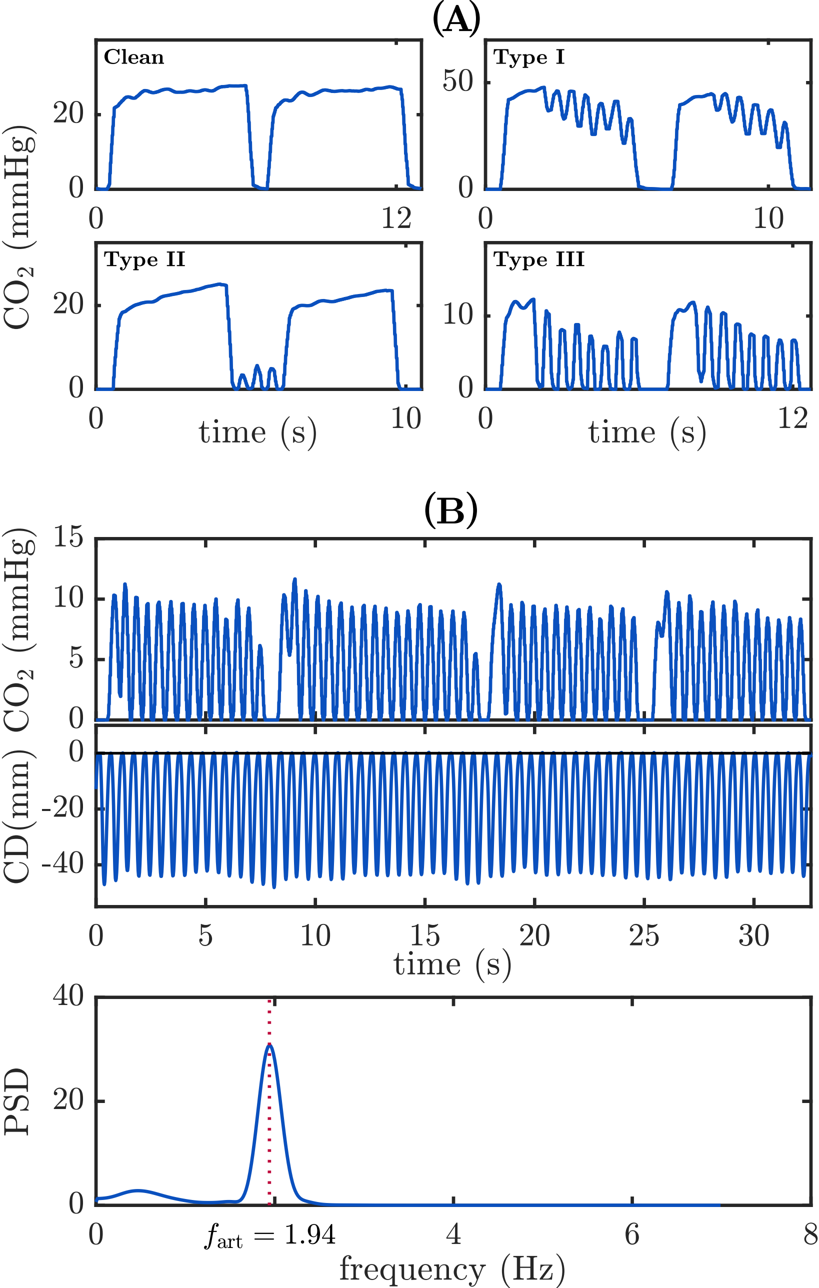
(A)
Clean
Type I
Type II
Type III
CO_2 (mmHg)
time (s)
(B)
CO_2 (mmHg)
CD(mm)
time (s)
PSD
$f_{\text{art}} = 1.94$
frequency (Hz)

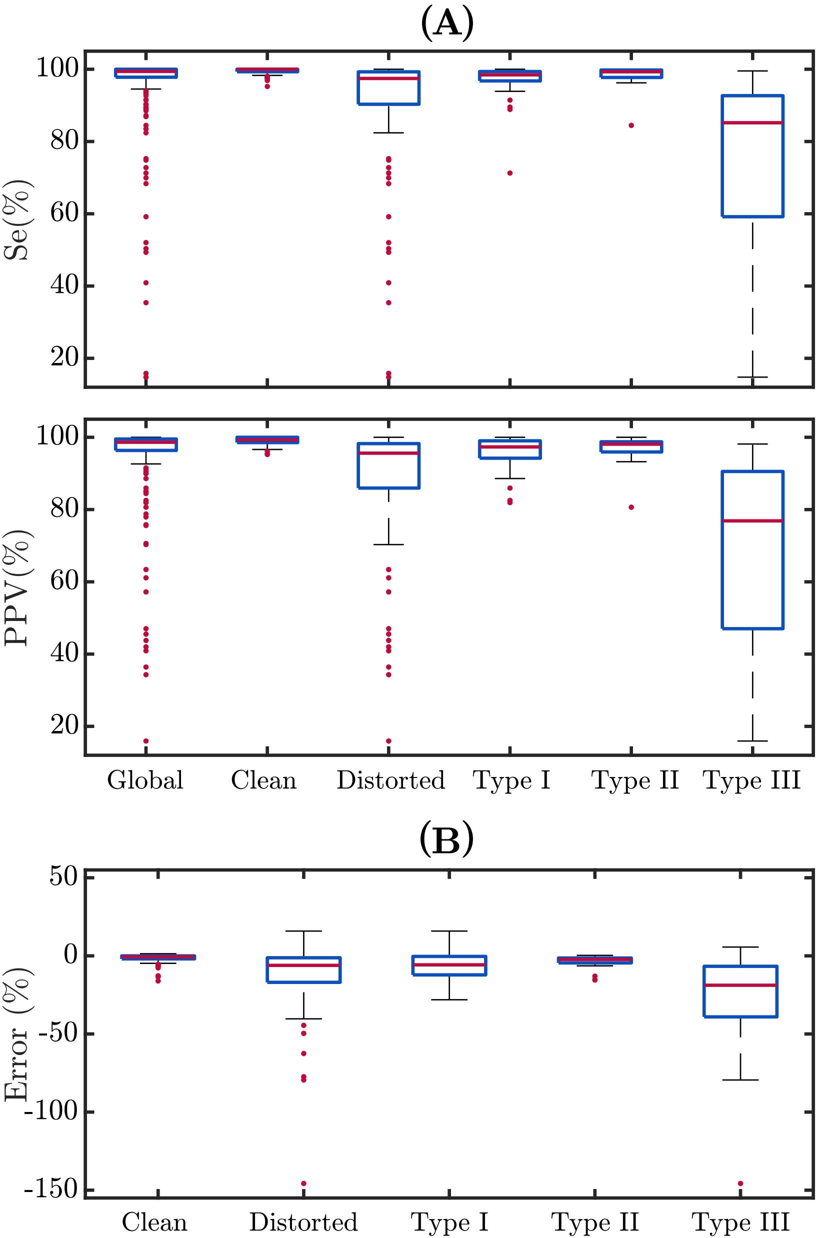

(A)
Se(%)
PPV(%)
100
80
60
40
20
Global
Clean
Distorted
Type I
Type II
Type III
(B)
Error (%)
50
0
-50
-100
-150
Clean
Distorted
Type I
Type II
Type III